REPORT DOCUMENTATION PAGE

Form Approved
OMB No. 0704-0188

1. AGENCY USE ONLY (Leave blank)	2. REPORT DATE	3. REPORT TYPE AND DATES COVERED
	October 1995	

4. TITLE AND SUBTITLE

Techniques for Determing Missile Roll Parameters from a Wind Tunnel

5. FUNDING NUMBERS

6. AUTHOR(S)

Ronald T. Wincey

7. PERFORMING ORGANIZATION NAMES(S) AND ADDRESS(S)

Defense Intelligence Agency
Missile & Space Intelligence Center
Redstone Arsenal, AL 35898-5500

8. PERFORMING ORGANIZATION REPORT NUMBER

MSC2-TM-95-001

9. SPONSORING/MONITORING AGENCY NAMES(S) AND ADDRESS(S)

N/A

10. SPONSORING/MONITORING AGENCY REPORT NUMBER

N/A

11. SUPPLEMENTARY NOTES

12a. DISTRIBUTION/AVAILABILITY STATEMENT

Approved for Public Release: distribution unlimited

12b. DISTRIBUTION CODE

13. ABSTRACT *(Maximum 200 words)*

A collection of the most prominent wind tunnel test techniques for determining missile aerodynamic roll parameters is presented. Both free-spin, and constrained-spin techniques are presented along with each techniques' advantages and disadvantages. Special consideration is given to showing how the model bearing friction can be automatically cancelled from the roll balance measurement by an internal electric spin-motor. This technique alleviates the need for special bearing-friction tare measurements.

14. SUBJECT TERMS

damping
roll
wind tunnel tests
free spin
constrained spin
spin motor
bearing friction

15. NUMBER OF PAGES

27

16. PRICE CODE

17. SECURITY CLASSIFICATION OF REPORT	18. SECURITY CLASSIFICATION OF THIS PAGE	19. SECURITY CLASSIFICATION OF ABSTRACT	20. LIMITATION OF ABSTRACT
UNCLASSIFIED	UNCLASSIFIED	UNCLASSIFIED	UNLIMITED

MSC2-TM-95-001

MSIC
TECHNICAL MEMORANDUM

Techniques for Determining Missile Roll Parameters from a Wind Tunnel

Author: Ronald T. Wincey

of
Ballistic Missile West Division
Offensive Systems Directorate
Missile and Space Intelligence Center
Defense Intelligence Agency

October 1995

ABSTRACT

A collection of the most prominent wind tunnel test techniques for determining missile aerodynamic roll parameters is presented. Both free-spin and constrained-spin techniques are presented along with each techniques' advantages and disadvantages. Special consideration is given to showing how the model bearing friction can be automatically cancelled from the roll balance measurement by an internal electric spin-motor. This technique alleviates the need for special bearing-friction tare measurements.

TABLE OF CONTENTS

NOMENCLATURE

C_l	Roll moment coefficient
C_{l_δ}	Roll moment coefficient due to fin cant, $\frac{\partial C_l}{\partial \delta}$
C_{l_p}	Roll damping coefficient, $\frac{\partial C_l}{\partial\left(\frac{pd}{2V}\right)}$
d	Reference length, model diameter
F_{MOG}	Motor-gear force
$F_{N_{B_T}}$	Total bearing normal force loading
F_{PGS}	Pinion-gear shaft lateral force
F_{RG}	Ring-gear force
$F_{Y_{PG}}$	Total pinion-gear force parallel to the Y-axis
I_x	Roll moment of inertia of the spinning mass
L_A	Aerodynamic roll moment, $C_{l_\delta} \delta qSd$
$L_{X_{BAL}}$	Model balance roll moment
L_{MBF}	Model bearing friction roll moment/torque
L_{MDT}	Motor driving torque
L_{MOG}	Motor-gear torque
L_{MOT}	Model motor roll torque
L_{oB}	Static bearing rolling moment at p=0
L_p	Roll damping moment per roll rate, $C_{l_p} \frac{qSd^2}{2V}$
L_{p_1}, L_{p_2}, L_{p_3}, L_{p_5}	Roll moment terms for the nonlinear equation of motion in roll
L_{PGBF}	Pinion-gear bearing friction torque
L_{ROTBF}	Rotor bearing friction torque
L_T	Total roll moment
$L_{\gamma\alpha}$	Roll moment with respect to roll position and angle of attack
M_X	Moments about the model X-axis

$M_{X_{BAL}}$	Moments about the balance X-axis
$M_{X_{PGS}}$	Moments about the pinion-gear shaft parallel to the X-axis
$M_{X_{ROT}}$	Moments about the rotor X-axis
M_∞	Free stream Mach number
p, $\dot{\Phi}$	Model roll rate
p_{ss}	Steady state roll rate
p_t	Vacuum tank pressure
$\dot{p}$, $\ddot{\gamma}$	Model roll acceleration
$\frac{pd}{2V}$	Roll rate parameter
q, Q	Dynamic pressure, $\frac{1}{2}\rho V^2$
Re_d	Free stream Reynolds number based on model diameter
r_{MOG}	Motor-gear radius
r_{PG}	Pinion-gear radius
r_{RG}	Radial distance from model centerline to ring gear
S	Reference Area
t	Time
t_1	Initial time
V	Tunnel test velocity
α	Angle of attack
Φ, γ	Model roll position
δ	Fin cant defection angle

LIST OF ILLUSTRATIONS

LIST OF TABLES

1. Introduction

The Gulf War reemphasized the importance of having accurate missile simulations when trying to understand the different factors that influence threat definition. For some missile systems, previous simulations have shown an extreme sensitivity to the equation-of-motion parameters used to describe free-flight missile roll and predict pitch-yaw-roll instability. Since input parameters are a main source of error for any simulation, substantial effort should be made to obtain the most accurate parameters possible. Therefore, it behooves the analyst to thoroughly investigate the parameters needed to accurately simulate all the related aspects of rolling motion and the best way to obtain these parameters.

In the process of investigating roll damping techniques, two related references[1,2] were found that implied wind tunnel model bearing friction could be cancelled from the roll balance measurement. This was possible through the use of an internal electric spin-motor. Since this was a unique technique that was not widely used, and a detail explanation was not given, further investigation was felt to be necessary.

2. Purpose

The purpose of this paper was originally to document the investigation of Ref. 1 & 2's implications. During the course of the documentation, the scope of this paper was broadened to include a presentation of the most prominent techniques used to determine all the aerodynamic parameters needed to simulate missile rolling motion.

In this paper, several techniques are presented with both advantages and disadvantages discussed. Also, since the availability and usage of a motor driven model from a previous MSIC test is believed to provide a cost savings, the technique using this type of equipment, as presented in Ref. 1, is analyzed. The results of this analysis are presented in the appendixes.

3. Background

From a review of roll damping wind tunnel test reports, it is apparent that roll damping is usually a derived parameter rather than directly measured. Roll damping, C_{l_p}, is defined as the rate of change of roll torque, C_l, with respect to the change of the roll rate parameter, $\frac{pd}{2V}$, or

$$C_{l_p} = \frac{\partial C_l}{\partial\left(\frac{pd}{2V}\right)} \tag{1}$$

where p is the model roll rate, d is the model reference diameter, and V is the tunnel test air velocity. The roll rate parameter can be shown to be the tangent of the effective angle of attack, induced by the

roll rate, occurring at the model reference diameter. The roll rate parameter is the scaling factor that must be matched with full scale conditions when determining the appropriate test conditions such as roll rate.

Roll damping has historically been derived using several techniques as discussed in Ref. 3. These techniques fall into two basic categories, i.e., free-spin and constrained-spin. Within the free-spin category, the technique also depends on whether the equation-of-motion about the model centerline is used during roll acceleration, $\dot{p} \neq 0$, or steady-state roll rate, $\dot{p} = 0$.

The following simplified equation-of-motion is usually used with these techniques.

$$I_x \dot{p} = L_T = L_A + L_p p \qquad (2)$$

where L_T is the total rolling moment, L_A is the aerodynamic roll moment due to fin cant, $C_{l_\delta} \delta qSd$, L_p is the aerodynamic roll damping moment per roll rate, $C_{l_p} \frac{qSd^2}{2V}$, and I_x is the moment of inertia of everything that is connected to the model and spinning about the model centerline. This equation is obtained by equating the rate of change of the angular momentum to the applied moments about the model centerline.

4. Free-Spin Technique

The free-spin technique includes all roll damping techniques that do not maintain a hard drive connection between the model and the support sting. This technique usually forces the model to spin up with deflected fins or a separate air drive. After spin-up, depending on the type of test, either a constant roll rate is maintained, the roll rate is allowed to change as the model is pitched, or the drive is disconnected and the model is allowed to spin down. The types of tests associated with this technique differ mainly upon when the data is acquired. The different periods of data acquisition associated with the different test types are (1) only during spin-up, (2) only during spin-up and steady-state, (3) only during steady-state, (4) only during spin-down, or (5) continuously throughout angle of attack sweeps. The only measured data needed to determine roll damping for all the test types except (3) are roll rate and/or roll position versus time. Test type (3) is a special case that needs only one or two steady-state roll rates to be measured. If only one steady-state roll rate is measured, then the static C_{l_δ} is also needed.

Several methods have been used to determine roll damping using the free-spin technique. The different methods are mostly variations of the same method that was changed when test objectives required a more accurate equation-of-motion.

4.1 Method 1

One method for determining roll damping and aerodynamic roll moment, as shown in Ref.'s 3 - 5, is obtained by integrating Eq. (2) with the initial conditions of $\dot{\Phi} = p = p_1$ at $t = t_1$ to give

$$\dot{\Phi} = p = \left(p_1 + \frac{L_A}{L_p}\right) e^{\frac{L_p}{I_x}(t - t_1)} - \frac{L_A}{L_p} \tag{3}$$

Substituting $\dot{p} = 0$ and $p = p_{ss}$ into Eq. (2) and solving for p_{ss}, gives

$$p_{ss} = -\frac{L_A}{L_p} \tag{4}$$

which is the steady-state roll rate. Substituting p_{ss} into Eq. (3) as well as the definition of L_p and solving for C_{l_p}, the following relationship is obtained.

$$C_{l_p} = \frac{I_x}{(t - t_1)} \ln\left(\frac{p - p_{ss}}{p_1 - p_{ss}}\right)\left(\frac{2V}{qSd^2}\right) \tag{5}$$

Then from Eq. (4)

$$C_{l_\delta} = -\frac{p_{ss} d}{\delta 2V} C_{l_p} \tag{6}$$

If I_x, p_{ss}, and two different (p,t) values are known, then C_{l_p} and C_{l_δ} can be calculated. Naturally, if p_{ss} is zero, then C_{l_δ} is zero and Eq. (5) reduces to

$$C_{l_p} = \frac{I_x}{(t - t_1)} \ln\left(\frac{p}{p_1}\right)\left(\frac{2V}{qSd^2}\right) \tag{7}$$

The above assumes, as Ref.'s 3 and 4 point out, (1) the system is exponentially damped, (2) the roll parameters are constant, and (3) there is no damping due to bearing friction. For the cases where these assumptions are approximately true, this technique has the advantage of obtaining the two roll parameters with a relatively small amount of effort. For the cases where the above assumptions are not approximately true, the above references suggest using Eq. (5) over small time intervals to obtain a locus of coefficients at average roll rates $(p_2 - p_1)/2$. Ref. 5 approaches the solution slightly different by fitting Eq. (3) to the measured (p,t) data using a differential-correction, least-squares curve-fit method to determine L_A and L_p.

In this method when bearing friction is significant, the bearing friction has to be subtracted from the overall roll damping derived from the curve-fitted roll rate data. Bearing friction can be determined in several ways. Traditionally it is determined, as in the above references, by evacuating the test section after every so many runs, spinning the model with an appropriate bearing load, and fitting the measured (p,t) data. The derived C_{l_p} from the evacuated test is assumed to be caused by bearing friction. The aerodynamic C_{l_p} is then determined by subtracting the evacuated C_{l_p} from the wind-on C_{l_p}.

Ref. 4 used this method with the Basic Finner model which is a cone-cylinder body with

rectangular tail fins. The following results were noted for spin rates of 50, 90, and 130 Hz:

At subsonic speeds (M_∞= 0.22 & 0.77):

1) C_{l_p} is highly dependent on spin rate and usually increases with spin rate.
2) From 0 to 10° angle of attack, C_{l_p} increases with angle of attack.
3) At M_∞ = 0.22 above 20° angle of attack, C_{l_p} mostly decreases with angle of attack.
4) At angles of attack above 60°, fin damping was the same order of magnitude as the bearing friction. When the evacuated readings were subtracted, the resulting data were unusable because of large data scatter.

At supersonic speeds:

1) C_{l_p} increases with angle of attack.
2) At M_∞ = 2.54, C_{l_p} increases slightly with spin rate up to 10° angle of attack. From 10 to 27°, C_{l_p} increases proportionally with spin rate.
3) At M_∞ = 4.1, C_{l_p} is independent of spin rate for the angles of attack of 0 to 20°.

4.2 Method 2

A second method, as shown in Ref. 6, for deriving roll damping and aerodynamic roll moment is to integrate Eq. (3) with the initial conditions $\Phi = \Phi_1$ at $t = t_1$ to obtain the following equation for roll position.

$$\Phi = \frac{\left(p_1 + \frac{L_A}{L_p}\right)}{\left(\frac{L_p}{I_x}\right)}\left[e^{\frac{L_p}{I_x}(t-t_1)} - 1\right] - \frac{L_A}{L_p}(t-t_1) + \Phi_1 \qquad (8)$$

Eq. (8) is then fitted to roll position versus time (Φ, t) data to determine L_A and L_p. The equation presented in Ref. 6, corresponding to Eq. (8), does not have the needed (L_p/I_x) denominator term. It is not known whether the omission occurred during the analysis or the reporting, but it is believed the omission would not substantially change Ref. 6's findings. Although not stated, it is believed Ref. 6 used the roll position equation instead of Eq. (3) because of the advantage that is derived from the double integration smoothing. The disadvantage of this method is the large amount of data that has to be taken. It was found by Ref. 6, Eq. (8) does not adequately describe the roll moment for subsonic speeds and high angles of attack over a large range of roll rates. This is believed to be because Eq. (8) is based on the same assumptions that pertained to Eq. (5). For subsonic speeds at high angles of attack, these assumptions are apparently not true. For these nonlinear areas of interest, the following equation was curve-fit to the (Φ, t) data using the technique described in Ref. 7.

$$I_x\dot{p} = L_A + L_{p_1}\dot{\Phi} + L_{p_2}\dot{\Phi}^2 + L_{p_3}\dot{\Phi}^3 + L_{p_5}\dot{\Phi}^5 \qquad (9)$$

Some data were found to be so nonlinear that even Eq. (9) was unable to produce a adequate fit. In those cases the data were broken into overlapping segments and Eq. (8) was fitted to each segment.

The bearing friction for this method was also determined by fitting the equation-of-motion to evacuated test section data, as well as data recorded from the rolling moment balance. Fig.'s 1-3 from Ref. 6 show the roll moment due to bearing friction increases with increasing roll rate, atmospheric pressure, and normal bearing load. Bearing friction moments from Ref. 8 agree with Ref. 6, and show for the higher bearing loads and roll rates less than 40 rad/sec, the bearing friction moment decreases with increasing roll rate. This trend is thought[8] to be caused by initial bearing stick. From 40 to 100 rad/sec, the bearing friction moment appears to be constant, but looking at Fig. 2, it seems to actually be the bottom of a slope reversal. Ref. 8 points out that although the balance roll moment actually reads the bearing friction, the value is usually smaller than the balance measurement uncertainty. While this is definitely a consideration, the majority of the data shown in Fig. 2 are above the balance measurement uncertainty of 0.003 ft-lb that was given in Ref. 6. All this points to the conclusion that bearing friction can be significant at higher roll rates and angles of attack.

The derivation that the roll moment balance actually reads the bearing friction when the model is spinning at a constant rate is shown in Appendix A. This also agrees with intuition when realizing if the model spins on frictionless bearings or air, there is no path available to transmit the roll moment to the balance. When bearing friction is added , the balance will sense and measure the friction torque, which in turn is equal to the imbalance between the aerodynamic driving and damping moments/torques.

Fig. 4 from Ref. 6 shows the areas of nonlinear roll damping derived using this method. Data are shown for both the Basic Finner and the Modified Basic Finner models at three different Reynolds numbers. The Modified Basic Finner is the Basic Finner except with an ogive nose and trapezoidal tail fins. Looking at Fig. 4, it is seen C_{l_p} is generally nonlinear at $M_\infty < 1.0$ and $\alpha > 20°$. Conversely, C_{l_p} is linear at $M_\infty < 2.0$ at $\alpha < 15°$ and at $M_\infty > 2.0$ at 0-90° angles of attack.

4.3 Method 3

A third method for determining roll damping, shown in Ref. 9, is to expand Eq. (2) to include a term for the induced roll moment as a function of angle of attack and roll angle. This extra term, shown in the following equation, came from the work of Nicolaides[10] while investigating bomb pitch-yaw-roll instabilities. This work concluded there is a periodic roll moment with respect to aerodynamic roll angle that increases with increasing angle of attack.

$$I_x\dot{p} = L_A + L_p p + L_{\gamma\alpha}\alpha\sin 4\gamma \qquad (10)$$

where γ is roll position.

The objective of Ref. 9 was to develop a more accurate mathematical description of single

degree-of-freedom rolling motion. The objective included trying to mathematically describe each of the nonlinear rolling characteristics such as "roll lockin", "roll breakout", and "roll speedup". As shown in the following equation, the induced rolling moment and roll damping moment require higher order terms to match the nonlinear rolling characteristics.

$$\ddot{\gamma} I_x / (QSd) = C_{l_\delta}(\alpha)\,\delta + \sum_{m,\,K} C_{l_{mK}}(\alpha)\,\dot{\gamma}^m \sin\left(4K\gamma + \tfrac{1}{2}m\pi\right) \qquad (11)$$

Also shown in the above equation is that the coefficients are a function of angle of attack. Eq. (11) was generalized by Ref. 11 to obtain the following equation which includes the mass and/or aerodynamic asymmetry terms.

$$\ddot{\gamma} = \frac{QSd}{I_x} \sum_{j=0}^{J} \left(\frac{\dot{\gamma} d}{2V}\right)^j \sum_{k=0}^{K} (C_{jk} \cos 4k\gamma + S_{jk} \sin 4k\gamma) + C_{ac} \cos\gamma + C_{as} \sin\gamma \qquad (12)$$

Table 1 from Ref. 12 shows the corresponding conventional coefficients of the coefficients in Eq. (12).

Similar to method 2, Eq. (12) is fitted to roll position vs. time, (γ,t), data using a "global" least-squares fitting procedure from Ref.'s 7 and 11. According to Ref. 13, bearing friction was not considered to be a significant factor for the tests that used this method. This was because a special, low-friction, gas bearing was used. This method has the disadvantage of having to take a large amount of data and time to extract the coefficients. It is the most extensive of the three free-spin methods and is the only method that includes the induced roll moment, roll damping moment, and fin cant roll moment as a function of roll angle at the higher orders.

Ref. 12 documents the use of this method on a number of configurations at low subsonic speeds and high angles of attack. It was found that $C_{l_{p(4\gamma)}}$, as well as C_{l_p}, were required to model the roll damping characteristics, especially at high angles of attack due to positive roll damping moments.

4.4 Method 4

A fourth method of determining roll damping is one that only uses the steady-state roll rate. This method uses Eq. (6) in the following form

$$C_{l_p} = -C_{l_\delta} \delta \frac{2V}{p_{ss} d}, \qquad (13)$$

where C_{l_δ} is the static value. This method can only be used if there is an aerodynamic driving torque such as fin cant. Also, non-static C_{l_δ} can be derived if the fin cant can be changed to obtain a second steady-state roll rate. Then both C_{l_p} and C_{l_δ} can be derived from two equations with two unknowns.

(U) This method has the advantage of not having to determine I_x, but the disadvantage of having to assume that C_{l_p} and C_{l_δ} are constant with roll rate and bearing friction is zero. This

method also assumes the induced roll moment included in Method 3 integrates to zero over a complete revolution[16].

5. Constrained-Spin Technique

The constrained-spin technique uses a direct drive connection between the sting and the model with the connection remaining intact throughout the test. This technique has been used in the past[1, 2,14,15] because of the special requirement to accurately maintain specific roll rates. The desired roll rate is achieved using an internal electric motor mounted on the sting in front of the balance. The motor shaft is connected directly or through reduction gears to the model. Fig. 5 from Ref. 1 is an example of a non-geared drive motor connection, and Fig. 6 from Ref. 14 is an example of a geared drive motor connection. Because of the associated moments of inertia of the motor rotor and gears, constant roll rates are used.

The constrained-spin technique with an internal electric motor has the unique advantage of cancelling the bearing friction from the balance reading. Ref. 1 states that it can be shown the roll moment balance measures the negative of the motor and bearing friction roll torque as shown in the following equation.

$$-L_{x_{BAL}} = L_{MOT} + L_{MBF} \tag{14}$$

This in turn is shown[1] to be equal to the external aerodynamic roll moments or

$$L_{x_{BAL}} = C_{l_\delta} \delta q S d + C_{l_p} p \frac{q S d^2}{2V} \tag{15}$$

This equation is then used in a similar way as Method 4 of the free-spin technique. Using two different spin rates, both C_{l_δ} and C_{l_p} are calculated from two equations with two unknowns.

While it is intuitive in Method 2 of the free-spin technique that the roll moment balance measures the bearing friction, it is not intuitive from Ref. 1 what influence the internal motor has on the roll balance measurement. Ref. 1 essentially states in order to go from Eq. (14) to Eq. (15), the motor torque has to equal the negative of the combined aerodynamic and bearing friction torques or

$$L_{MOT} = -\left(C_{l_\delta} \delta q S d + C_{l_p} p \frac{q S d^2}{2V} + L_{MBF} \right) \tag{16}$$

This means the internal motor cancels the bearing friction from the roll moment balance. Ref. 15 alludes to this conclusion by finding in a lab test, using a configuration similar to Ref. 1, the balance at normal room conditions showed no effect of spin over the range of spin rates tested (-300 to 1575 rpm). This is contrary to what Fig. 1 from Ref. 6 shows from a free-spin test. Ref. 15 caveated this by noting the lab tests were conducted with no load on the model and the effect of bearing friction might become more apparent when the model is subjected to high normal-force loads. It is obvious that Ref. 15 did not believe the internal motor was cancelling the bearing friction.

The validity of Ref. 1's statements is shown by derivation in Appendix B. In this derivation, no gears are used and the motor is assumed to be turning in the same direction as the model. It is seen in Appendix B at a steady-state roll rate, the motor torque is equal to the combined torques of aerodynamics, model bearing friction, and motor bearing friction. When this is added to what the roll balance is reading, it is seen that all the friction torques cancel leaving only the aerodynamic torques. This means in the absence of aerodynamic roll driving moments, the roll balance will be directly measuring aerodynamic roll damping C_{l_p}. It also means this technique has an advantage in tests where the bearing friction could be changing significantly due to changing bearing loads, such as in high angle of attack sweeps.

In the geared configuration, Fig. 6, an intermediate pinion gear is used for torque amplification. The intermediate gear causes the model to turn in the opposite direction as the motor. The added gear bearing friction and gear attachment loads, along with the question of whether the motor-turning direction is a significant factor, led to doubt as to Ref. 1's applicability to the geared motor configuration. Appendix C shows the internal motor in the geared configuration also compensates for the model and gear bearing friction resulting in the roll moment balance measuring only the external aerodynamic roll moments.

In addition to the advantage of bearing friction cancellation, this technique has the same advantage as Method 4 of the free-spin technique of not having to determine I_x because it operates at steady-state roll. It also has the same disadvantages as Method 4 of having to assume both C_{l_p} and C_{l_δ} are constant with roll rate. Naturally, the constrained-spin technique also has the disadvantage of not being able to investigate nonlinear free-spinning phenomena such as "roll lockin", "roll breakout", and "roll speedup" as discussed in Method 3.

6. Combination of Techniques

Obviously the ideal situation would be to combine the advantages of the friction compensation technique with the least-squares curve-fitting technique (Method 3) that provides the induced roll, roll damping, and roll driving moments as a function of roll position and angle of attack. Several things should be considered when this is attempted. As in Methods 2 and 3 of the free-spin technique, high data rates will be required that are not filtered. Also prior to testing, the balance should be checked to see if the rotor pulses are contaminating the roll balance readings. If they are, hopefully the pulses can be filtered out without affecting the desired data.

7. Conclusions

The conclusions derived from this investigation are:

1) An internal electric motor can be used to cancel the model bearing friction read by the roll balance.

2) The simplified one-degree-of-freedom equation-of-motion is not adequate to derive the roll damping coefficient at subsonic speeds and high angles of attack.

3) There is a possibility that the induced rolling moment and higher-order roll damping coefficients are needed to model rolling motion at supersonic speeds and high angles of attack.

References

1. Fernandes, F. D., "RAM HSWT-705 Wind Tunnel Test Report, Rolling/Controlling Model," GDP TM 6-332-101.53-23, March 1985.

2. Tisserand, L. E., "Aerodynamics of a Rolling Airframe Missile," JHU/APL (ADA111769), May 1981.

3. Schueler, C. J., Ward, L. K., Hodapp, A. E., Jr., "Techniques for Measurements of Dynamic Stability Derivatives in Ground Test Facilities," AGARDograph 121 (AD669227), October 1967.

4. Regan, F. J., "Basic Damping Moment Measurements for the Basic Finner at Subsonic and Supersonic Speeds," NAVORD Rpt. 6652, March 1964.

5. Helmlinger, K. R. and Jenke, L. M., "Experimental Static Stability, Pressure, Roll-Damping, and Three-Degree-of-Freedom Characteristics of Recovered Ablated Nose Tips at Mach Numbers 2, 4, and 5," AEDC-TR-77-14 (ADB017482), March 1977.

6. Jenke, L. M., "Experimental Roll-Damping, Magnus, and Static-Stability Characteristics of Two Sender Missile Configurations at High Angles of Attack (0 to 90 Deg) and Mach Numbers 0.2 Through 2.5," AEDC-TR-76-58 (ADA027027), July 1976.

7. Chapman, G. T. and Kirk, D. B., "A New Method for Extracting Aerodynamic Coefficients from Free-Flight Data," AIAA Journal, Vol. 8, No. 4, April 1970.

8. Marquart, E. J., "Free-Spin Damping Measurement Techniques," AIAA Paper 93-3457-CP.

9. Daniels, P., "A Study of the Nonlinear Rolling Motion of a Four-Finned Missile," Journal of Spacecraft and Rockets, Vol. 7, No. 4, April 1970.

10. Nicolaides, J. D., "On the Rolling Motion of Missiles," Bureau of Ordnance BTN 33 (ADB962032), March 1957.

11. Cohen, C. J. and Clare, T. A., "Analysis of the Rolling Motion of Finned Missiles," NWL

Technical Report TR-2671, NSWC/DL, February 1972.

12. Daniels, P. and Hardy, S., "Theoretical and Experimental Methods in the Solution of Missile Nonlinear Roll Problems," NSWC /DL TR-3773 (ADA055718), March 1978.

13. Hardy, S., NSWC, Telephone conversation, 9/12/95.

14. Auman, L. M. and Winn, G. C., "Wind Tunnel Investigation of a Spinning Missile with Active Canard Control," AIAA Paper 94-0722.

15. Uselton, J. C., "Force Tests on a Spinning TX-61 Model at M_∞ = 2.0, 2.5, and 3.0," AEDC-TR-65-10 (AD454931), January 1965.

16. Fernandes, D., Telephone conversation, 11/21/95.

Table 1. Aerodynamic Roll Moment Coefficient Correlation*

Coefficient		
Conventional Nomenclature	Computer Program Nomenclature	Description
$C_{l_{\delta}}{}^{\delta}$	C_{00}	Fin cant roll moment coefficient
$C_{l_{\delta(4\gamma)}}{}^{\delta}$	C_{01}	Variation of fin cant moment coefficient with roll angle
$C_{l_{\delta(8\gamma)}}{}^{\delta}$	C_{02}	
$C_{l_{\delta(12\gamma)}}{}^{\delta}$	C_{03}	
.	.	
.	.	
.	.	
$C_{l_{\delta(4K\gamma)}}{}^{\delta}$	C_{0K}	
C_{l_p}	C_{10}	Linear roll damping moment coefficient derivative
$C_{l_{p^2}}$	C_{20}	Quadratic roll damping moment coefficient derivative
$C_{l_{p^3}}$	C_{30}	Cubic roll damping moment coefficient derivative
.	.	
.	.	
.	.	
$C_{l_{p^J}}$	C_{J0}	
$C_{l_{p(4\gamma)}}$	C_{11}	Variation of linear roll damping moment coefficient derivative with roll angle
$C_{l_{p(8\gamma)}}$	C_{12}	
$C_{l_{p(12\gamma)}}$	C_{13}	
.	.	
.	.	
.	.	
$C_{l_{p(4K\gamma)}}$	C_{1K}	
$C_{l_{(4\gamma)}}$	S_{01}	Induced rolling moment coefficients
$C_{l_{(8\gamma)}}$	S_{02}	
$C_{l_{(12\gamma)}}$	S_{03}	
.	.	
.	.	
.	.	
$C_{l_{(4K\gamma)}}$	S_{0K}	
	C_{ac}	Roll asymmetry coefficients (Combinations of aerodynamic and mass asymmetry constants)
	C_{as}	

*All coefficients are a function of the missile's angle of attack.

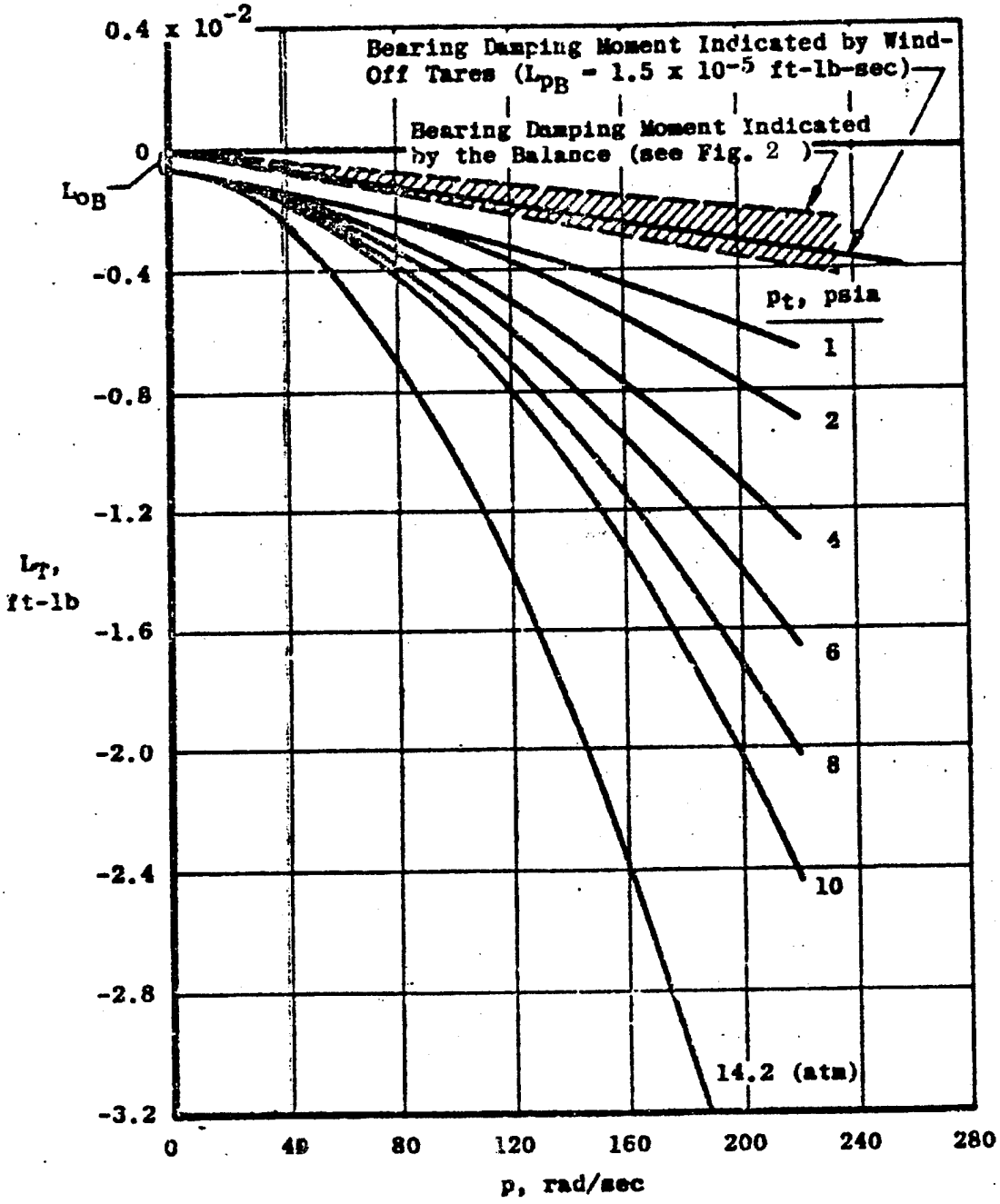

Figure 1. Model-bearing system total rolling moment

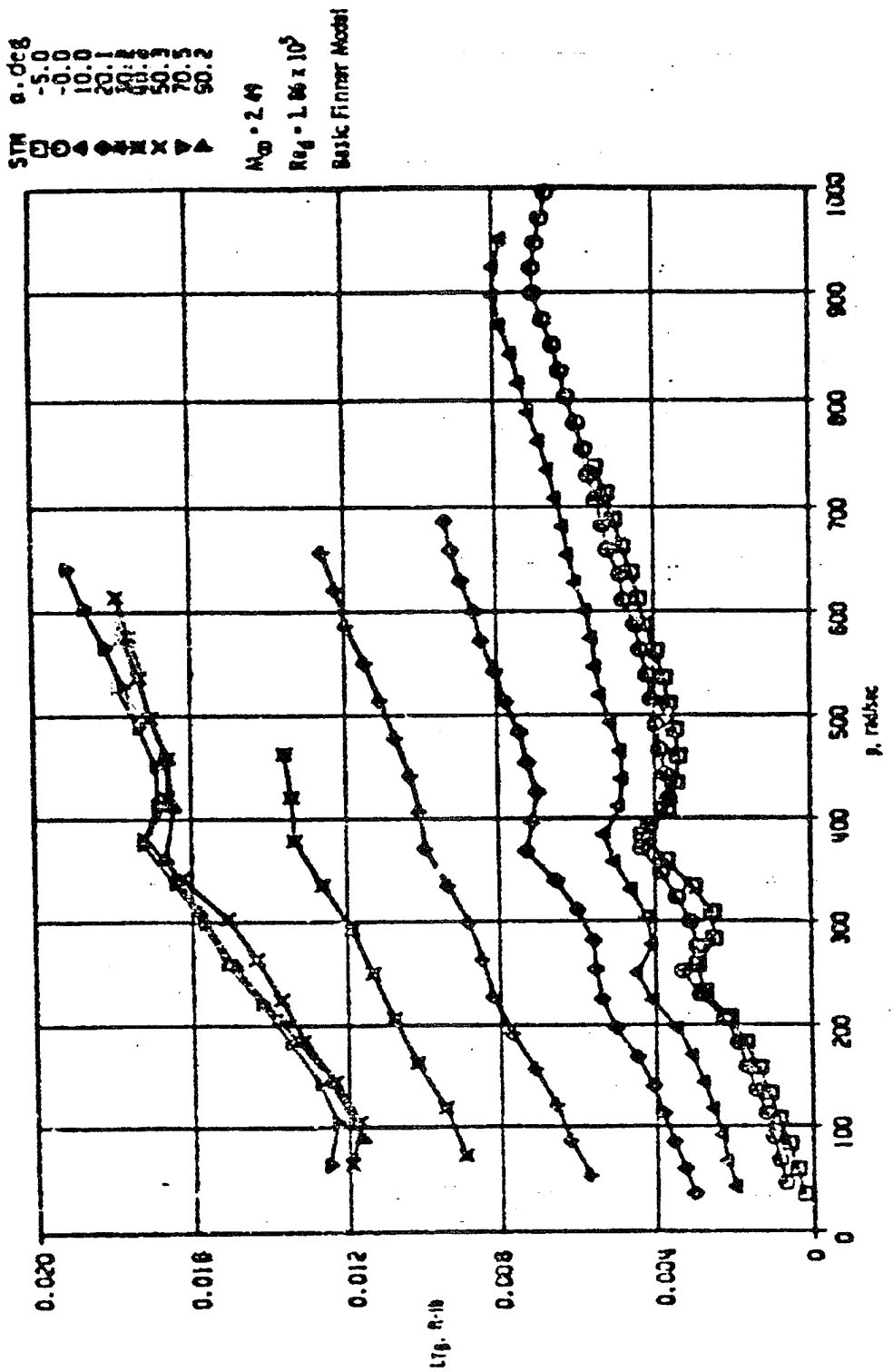

Figure 2. Total-bearing moment measured by the balance

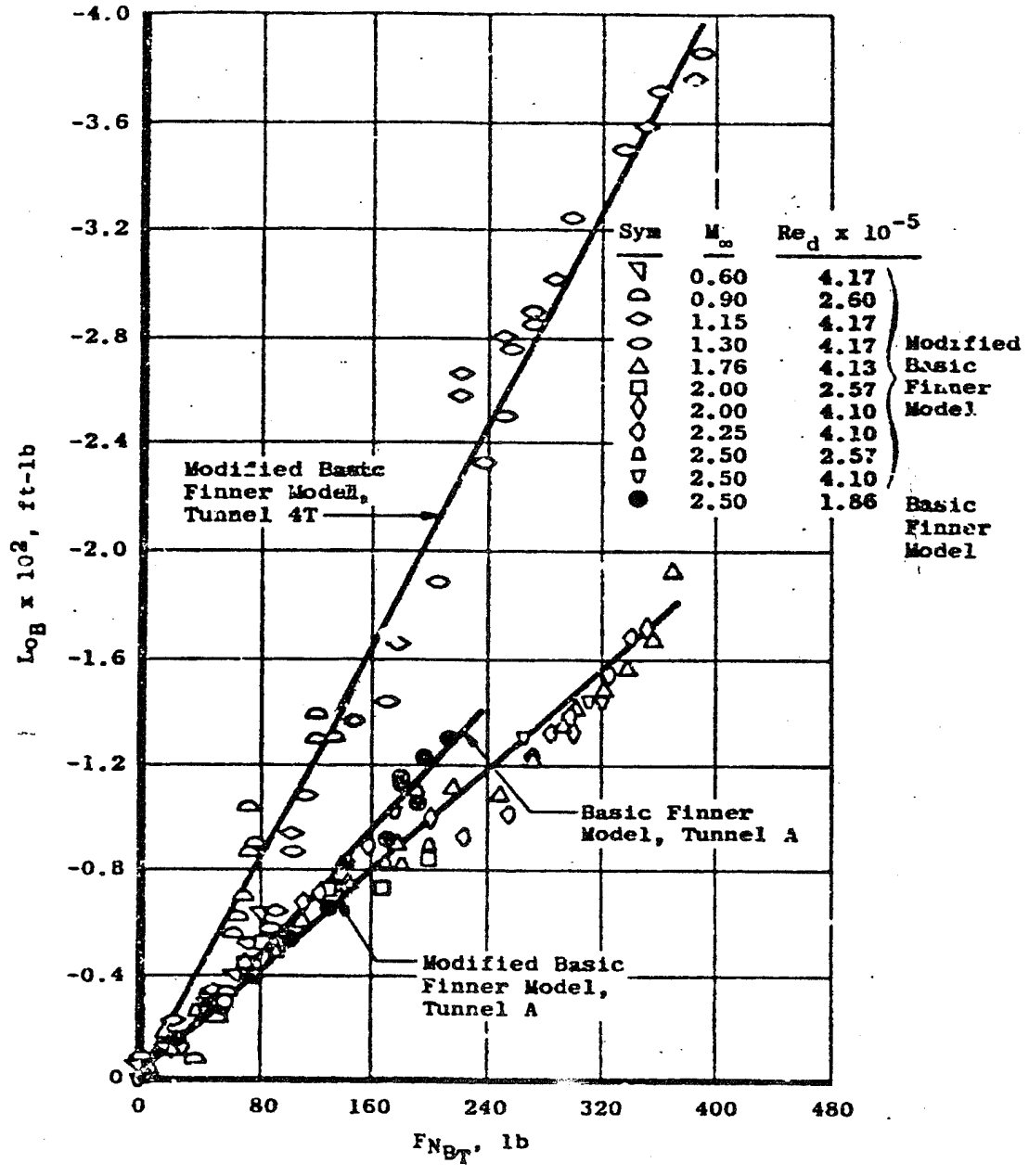

Figure 3. Variations of bearing static rolling moment with load

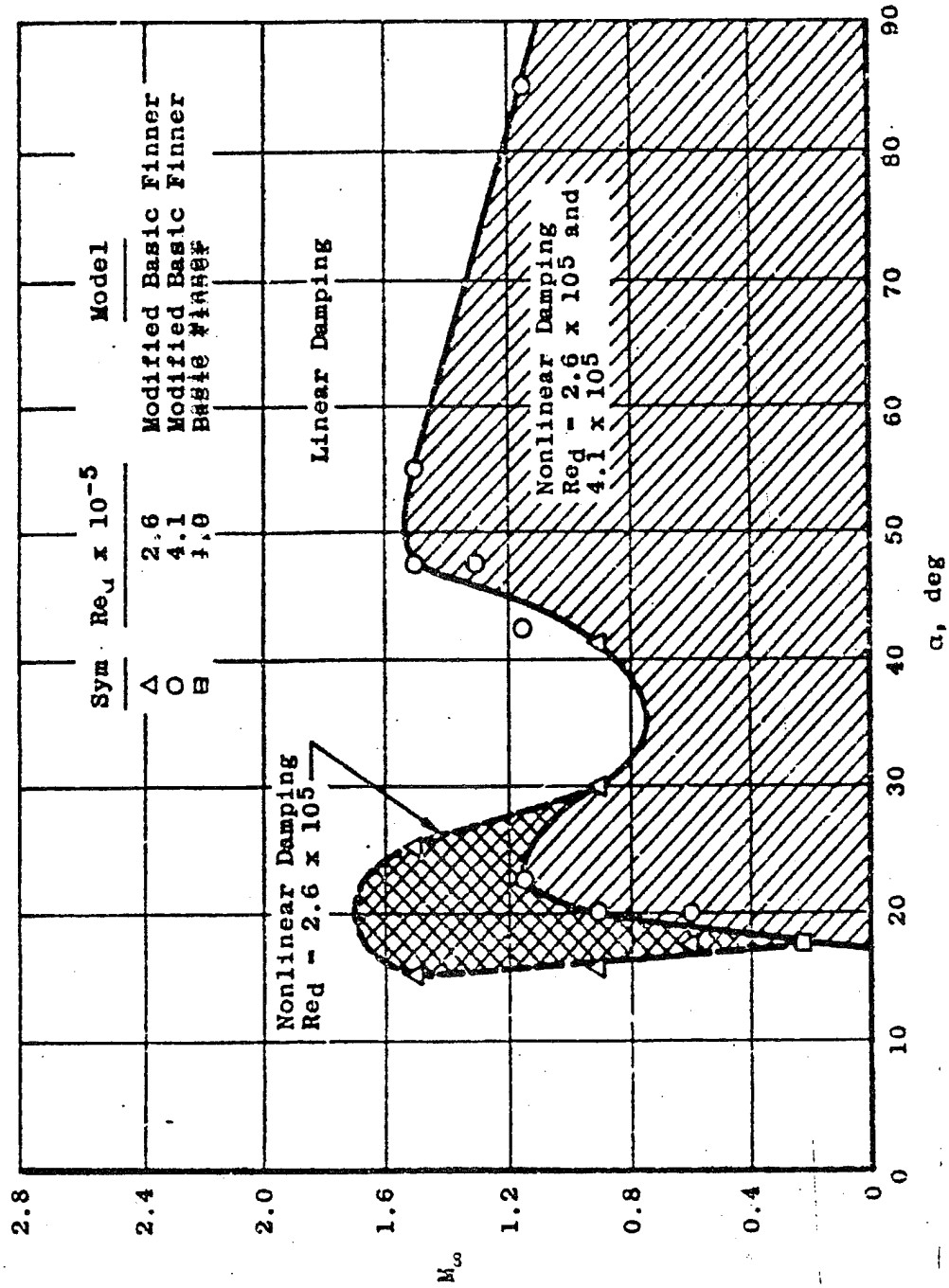

Figure 4. Approximate region of nonlinear damping

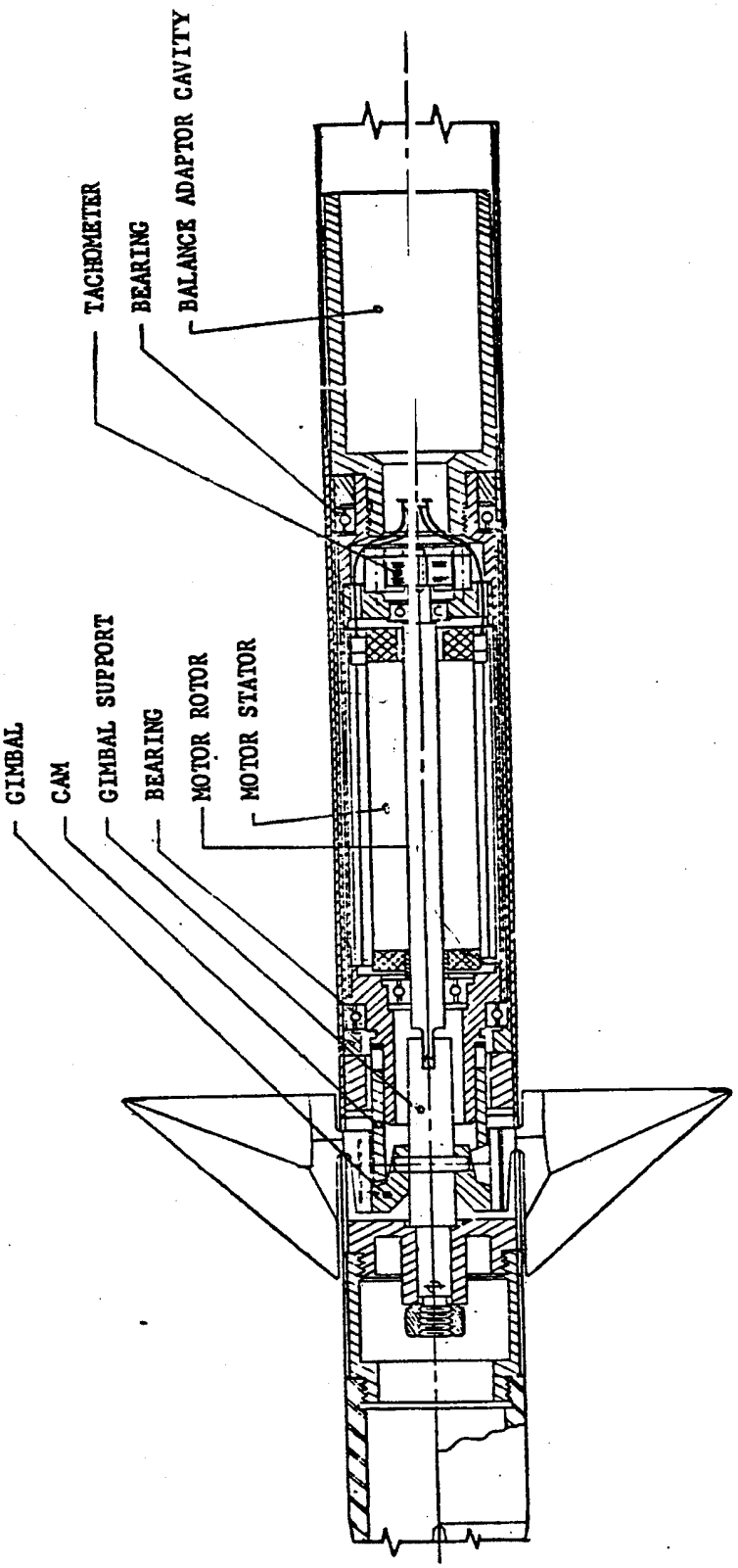

Figure 5. Non-geared spin-motor model

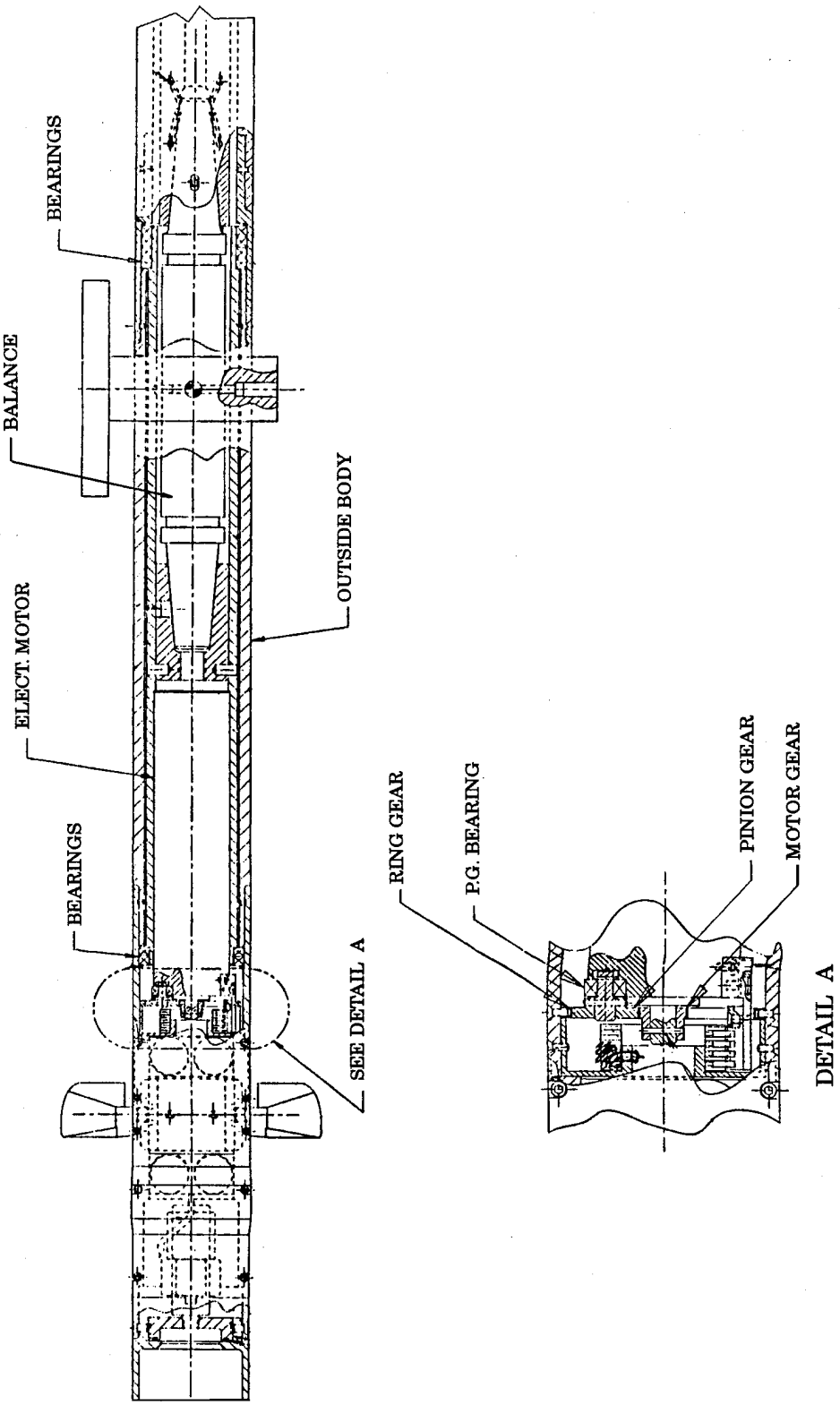

Figure 6. Geared spin-motor model

Appendix A

Derivation of the Roll Balance Reading on a Free-Spin Model

(U) For the case of a free spinning model, a free body diagram (Fig. A1) can be used to show all the roll moments that influence rolling motion. If it is assumed the model is spinning at a constant roll rate at a small angle of attack, and the aerodynamic damping and bearing friction are acting in the opposite direction as the driving torque; the following equation is true.

$$\curvearrowright \sum M_x = 0 = C_{l_\delta} \delta q S d - C_{l_p} p \frac{q S d^2}{2V} - 2L_{MBF} \qquad \text{(A1)}$$

where L_{MBF} is the model bearing friction moment.

Therefore, the bearing friction moment is equal to the difference of the aerodynamic driving and damping moments or

$$2L_{MBF} = C_{l_\delta} \delta q S d - C_{l_p} p \frac{q S d^2}{2V} \qquad \text{(A2)}$$

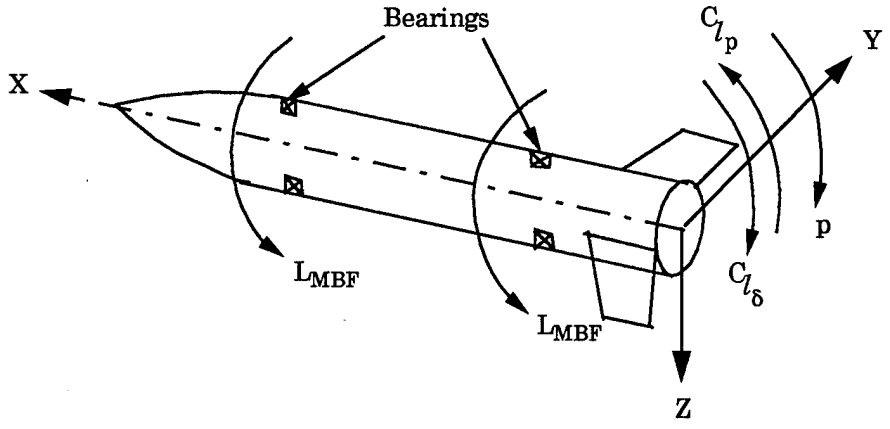

Figure A1. Free-spin-model free body

(U) Looking at the free body of the balance inside the spinning model (Fig. A2) and realizing the bearing friction moment is acting in the opposite direction on the bearing adapter as it was on the model, it is seen the following is also true.

$$\sum M_{x_{BAL}} = 0 = 2L_{MBF} + L_{x_{BAL}} \tag{A3}$$

Therefore,

$$-L_{x_{BAL}} = 2L_{MBF} \tag{A4}$$

and from Eq. A2

$$-L_{x_{BAL}} = C_{l_\delta} \delta q S d - C_{l_p} p \frac{qSd^2}{2V} \tag{A5}$$

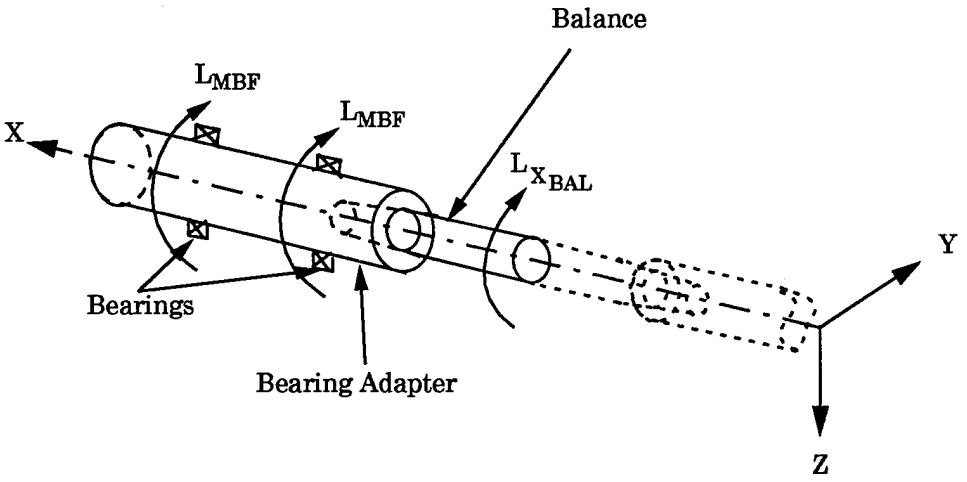

Figure A2. Bearing-adapter/balance free body

Appendix B

Derivation of the Roll Balance Reading on a Constrained-Spin Model that is Directly Connected to the Spin Motor

(U) For the case of a constrained-spin model with the motor shaft connected to the model (Fig. 5), a free body (Fig. B1) can be used to show the roll moments acting on the model that cause the model to roll. The following equation assumes the model is rolling at a constant rate at a small angle of attack, and the aerodynamic damping and bearing friction torques are in the opposite direction as the motor and aerodynamic driving torques. The summation of the roll moments are

$$\sum M_x = 0 = C_{l_\delta} \delta q S d - C_{l_p} p \frac{q S d^2}{2V} + L_{MDT} - 2L_{MBF} \qquad \text{(B1)}$$

where L_{MBF} is the model bearing friction torque. From Eq. (B1), the motor driving torque is

$$L_{MDT} = C_{l_p} p \frac{q S d^2}{2V} - C_{l_\delta} \delta q S d + 2L_{MBF} \qquad \text{(B2)}$$

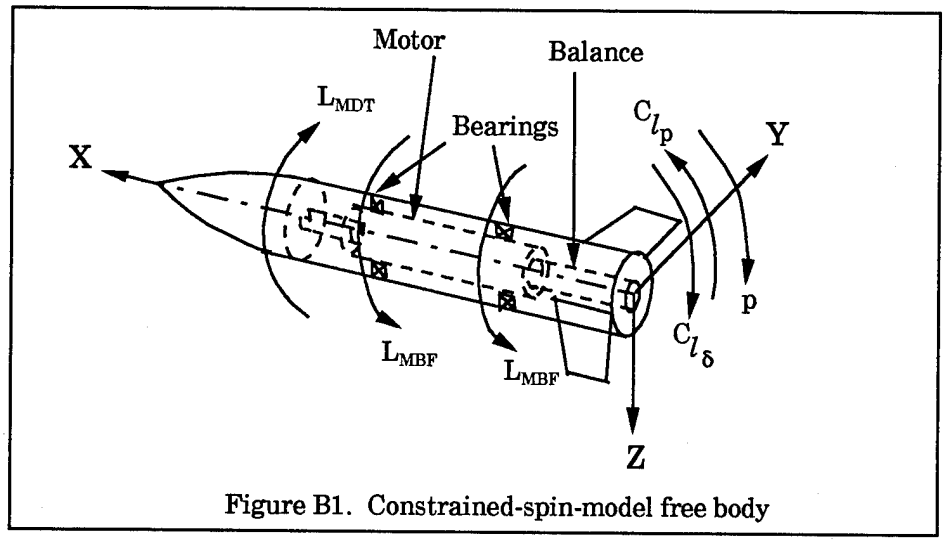

Figure B1. Constrained-spin-model free body

(U) Realizing the motor driving torque, L_{MDT}, is acting in the opposite direction on the rotor shaft as shown in Fig. B1, and the rotor bearing friction torque, L_{ROTBF}, is in the opposite direction as the rotor torque, the free body of the motor rotor is defined as shown in Fig. B2. Utilizing Fig. B2, the summation of torques on the rotor is

$$\sum M_{X_{ROT}} = 0 = L_{MOT} - 2L_{ROTBF} - L_{MDT} \qquad \text{(B3)}$$

From Eq. (B3), the motor torque is

$$L_{MOT} = L_{MDT} + 2L_{ROTBF} \tag{B4}$$

Substituting Eq. (B2) into Eq. (B4), it is seen the motor torque is equal to the aerodynamic and bearing friction torques.

$$L_{MOT} = C_{l_p} p\frac{qSd^2}{2V} - C_{l_\delta} \delta qSd + 2L_{MBF} + 2L_{ROTBF} \tag{B5}$$

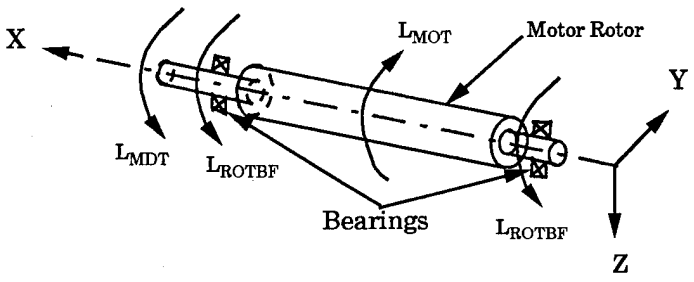

Figure B2. Motor rotor free body

(U) From the free body of the motor and the balance (Fig. B3), the summation of the torques are

$$\sum M_{X_{BAL}} = 0 = L_{X_{BAL}} - L_{MOT} + 2L_{ROTBF} + 2L_{MBF} \tag{B6}$$

The torques shown in Fig. B3 are in the opposite direction as shown in Fig.'s B1 and B2 because they are reactions. From the following equation, it is seen the balance is reading the difference between the motor torque and the bearing friction torques.

$$L_{X_{BAL}} = L_{MOT} - 2L_{ROTBF} - 2L_{MBF} \tag{B7}$$

By substituting Eq. (B5) into Eq. (B7), the following equation shows the motor torque cancels the bearing friction torque read by the balance.

$$L_{X_{BAL}} = C_{l_p} p\frac{qSd^2}{2V} - C_{l_\delta} \delta qSd + 2\cancel{L_{MBF}} + 2\cancel{L_{ROTBF}} - 2\cancel{L_{ROTBF}} - 2\cancel{L_{MBF}} \tag{B8}$$

Therefore, the balance is reading the negative of the aerodynamic roll moment minus the damping moment for the case of small angles of attack and constant roll rate.

$$-L_{X_{BAL}} = C_{l_\delta} \delta qSd - C_{l_p} p\frac{qSd^2}{2V} \tag{B9}$$

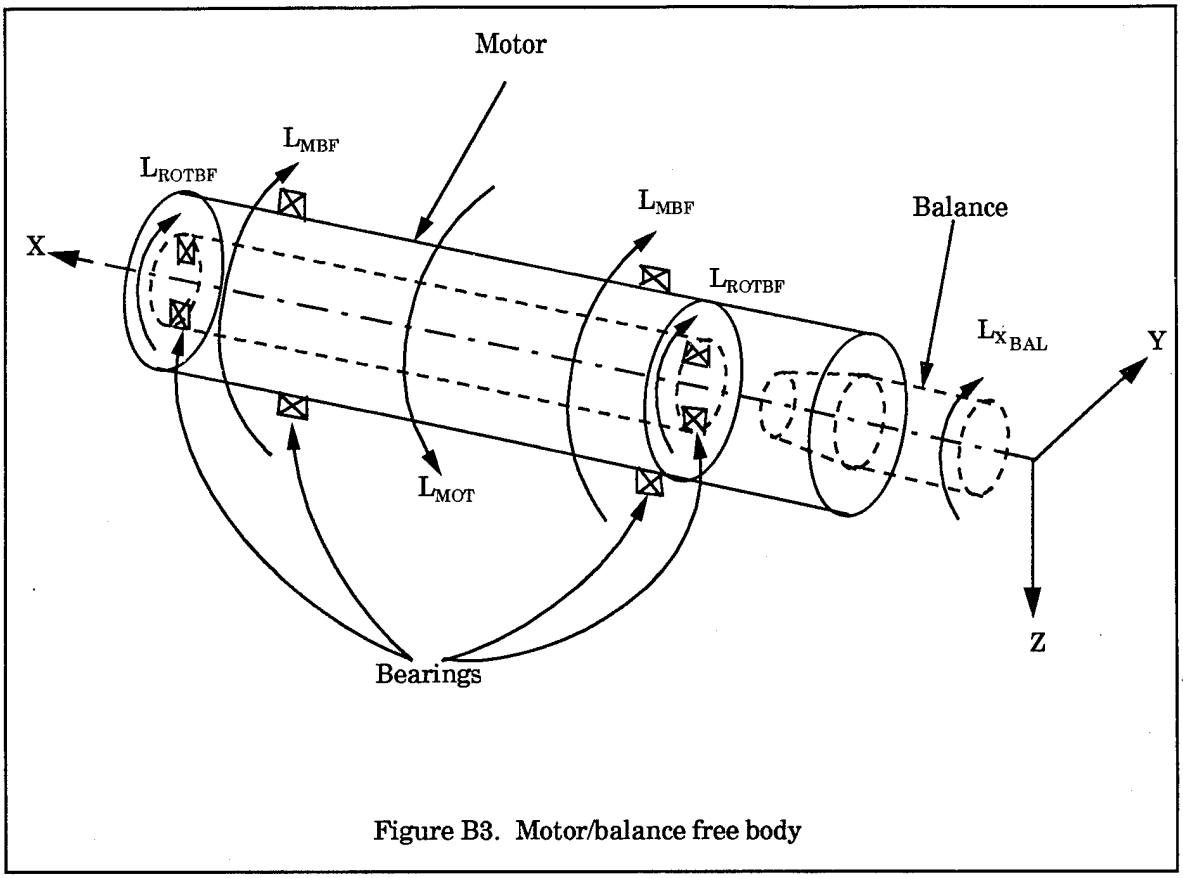

Figure B3. Motor/balance free body

Appendix C

Derivation of the Roll Balance Reading on a Constrained-Spin Model that is Directly Connected to the Spin Motor Through a Reduction Gear

(U) For the case of a constrained-spin model with the motor shaft connected to the model through a reduction gear (Fig. 6), a free body (Fig. C1) can be used to show the roll moments acting on the model that cause the model to roll. The following equation assumes the model is rolling at a constant rate at a small angle of attack, and the aerodynamic damping and bearing friction torques are in the opposite direction as the motor and aerodynamic driving torques. The summation of the roll moments are

$$\sum M_x = 0 = C_{l_\delta} \delta q S d - C_{l_p} p \frac{q S d^2}{2V} + F_{RG} r_{RG} - 2L_{MBF} \qquad \text{(C1)}$$

where F_{RG} is the pinion gear force applied to the ring gear, r_{RG} is the moment arm from the model centerline to the ring-pinion gear contact point, and L_{MBF} is the model bearing friction torque.

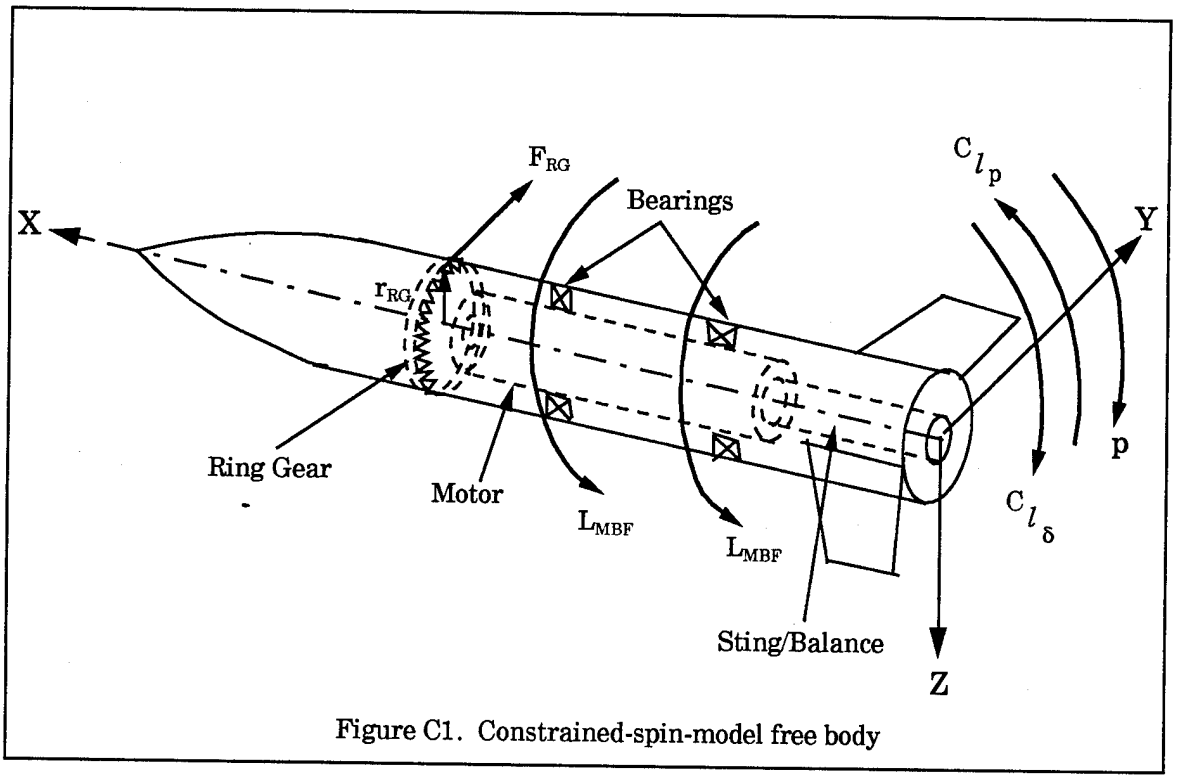

Figure C1. Constrained-spin-model free body

From Eq. (C1), the ring gear torque is

$$F_{RG} r_{RG} = C_{l_p} p \frac{qSd^2}{2V} - C_{l_\delta} \delta qSd + 2L_{MBF} \tag{C2}$$

which becomes

$$F_{RG}\left(r_{MOG} + 2r_{PG}\right) = C_{l_p} p \frac{qSd^2}{2V} - C_{l_\delta} \delta qSd + 2L_{MBF} \tag{C3}$$

where from Fig. C2,

$$r_{RG} = r_{MOG} + 2r_{PG}. \tag{C4}$$

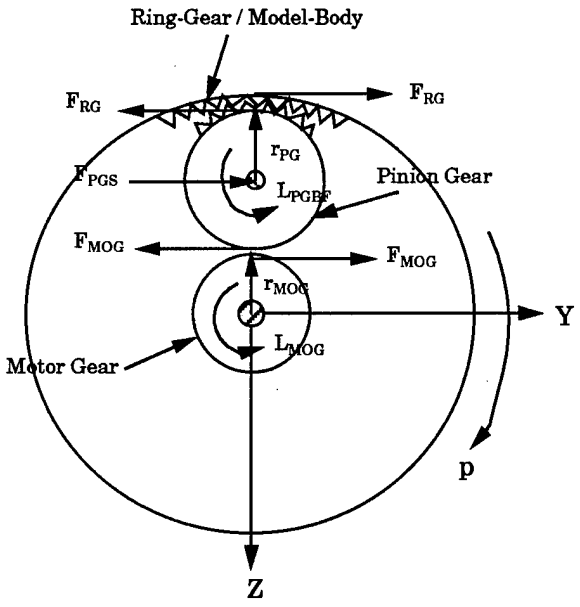

Figure C2. Model/gear free body

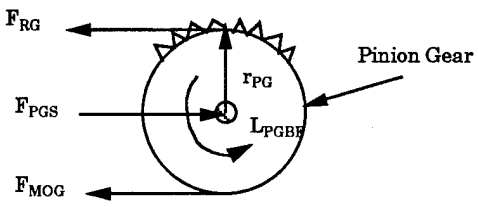

Figure C3. Pinion gear free body

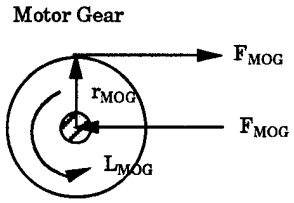

Figure C4. Motor gear free body

From the free body of the pinion gear, Fig. C3, the summation of forces in the Y direction yields

$$\sum F_{Y_{PG}} = 0 = -F_{RG} - F_{MOG} + F_{PGS} \tag{C5}$$

From the above equation, the side force on the pinion gear shaft is

$$F_{PGS} = F_{RG} + F_{MOG} \tag{C6}$$

which is acting at

$$r_{PGS} = r_{MOG} + r_{PG} \tag{C7}$$

from the motor centerline.

Also from Fig. C3, the summation of the moments about the gear shaft are

$$\sum M_{X_{PGS}} = 0 = F_{MOG}r_{PG} - F_{RG}r_{PG} - L_{PGBF} \tag{C8}$$

where L_{PGBF} is the pinion gear bearing friction torque. From Eq. (C8), the torque applied to the pinion gear is

$$F_{MOG}r_{PG} = F_{RG}r_{PG} + L_{PGBF} \tag{C9}$$

Looking at Fig. C4, the torque on the motor gear is

$$L_{MOG} = F_{MOG}r_{MOG} \tag{C10}$$

Just as in Appendix B, except the torques are in the opposite direction, the summation of the torques on the motor rotor, from Fig. C5, are

$$\sum M_{X_{ROT}} = 0 = -L_{MOT} + 2L_{ROTBF} + L_{MOG} \tag{C11}$$

and the motor torque is

$$L_{MOT} = L_{MOG} + 2L_{ROTBF} \tag{C12}$$

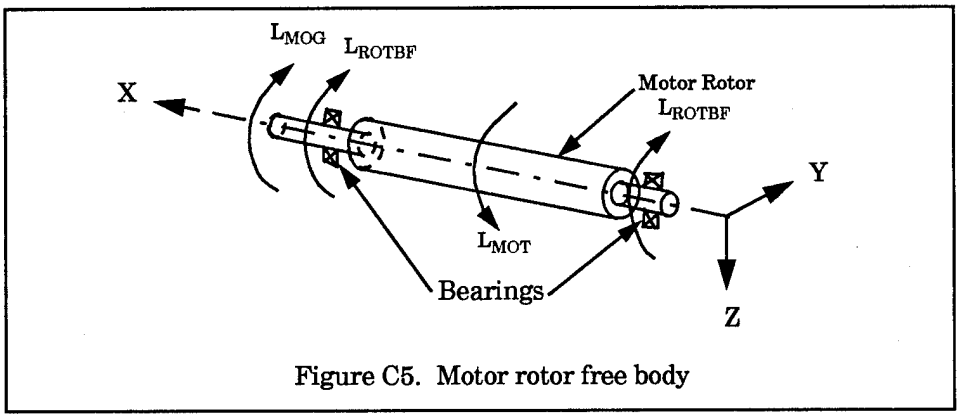

Figure C5. Motor rotor free body

Substituting Eq. (C10) into Eq. (C12) and using Eq.'s (C6) and (C7), the following is obtained

$$L_{MOT} = F_{MOG}r_{MOG} + 2L_{ROTBF} \tag{C13}$$

$$= (F_{PGS} - F_{RG})(r_{PGS} - r_{PG}) + 2L_{ROTBF} \tag{C14}$$

$$= F_{PGS}r_{PGS} - F_{RG}r_{PGS} - F_{PGS}r_{PG} + F_{RG}r_{PG} + 2L_{ROTBF} \tag{C15}$$

$$= F_{PGS}r_{PGS} - F_{RG}(r_{MOG} + r_{PG}) - (F_{RG} + F_{MOG})r_{PG} + F_{RG}r_{PG} + 2L_{ROTBF} \tag{C16}$$

$$= F_{PGS}r_{PGS} - F_{RG}(r_{MOG} + 2r_{PG}) - F_{MOG}r_{PG} + F_{RG}r_{PG} + 2L_{ROTBF} \tag{C17}$$

Therefore by substituting in Eq.'s (C3) and (C9) into Eq. (C17), the motor torque is

$$L_{MOT} = F_{PGS}r_{PGS} + C_{l_\delta}\delta qSd - C_{l_p}p\frac{qSd^2}{2V} - 2L_{MBF} - L_{PGBF} + 2L_{ROTBF} \qquad (C18)$$

which is the summation of the aerodynamic, bearing friction, and pinion-gear-reaction torques. Using Fig. C6 and realizing the forces and moments are reactions to the forces and moments in the previous figures, the summation of the moments about the balance centerline is

$$\sum \overset{\frown}{M_{X_{BAL}}} = 0 = L_{MOT} + 2L_{MBF} + L_{PGBF} - F_{PGS}r_{PGS} + L_{X_{BAL}} - 2L_{ROTBF} \qquad (C19)$$

Solving for the $-L_{X_{BAL}}$ and substituting for L_{MOT} from Eq. (C18), it is seen the roll moment balance reading is

$$-L_{X_{BAL}} = C_{l_\delta}\delta qSd - C_{l_p}p\frac{qSd^2}{2V} \qquad (C20)$$

This shows, just as in Appendix B, the motor torque is cancelling all torques except the aerodynamic roll moments when the model is at a constant roll rate.

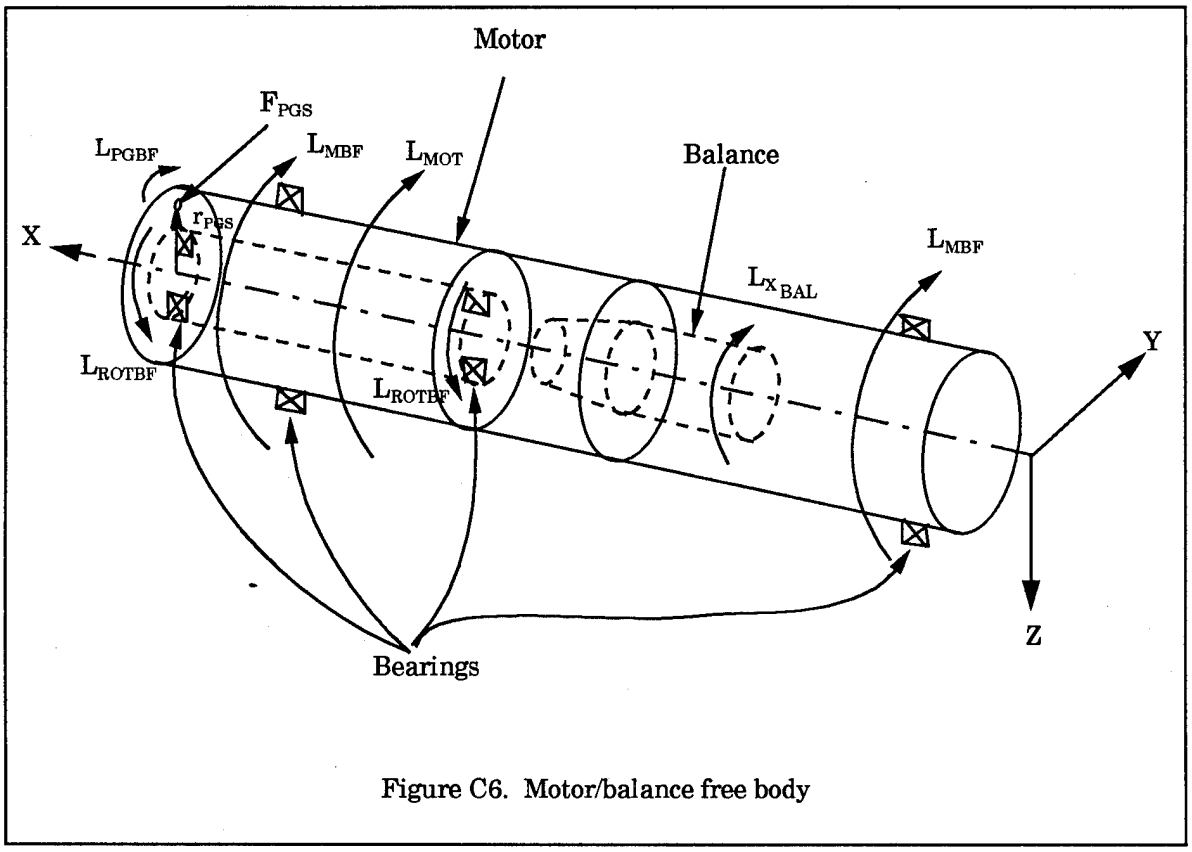

Figure C6. Motor/balance free body